Inorganic Chemistry

Article

pubs.acs.org/IC

Synthesis and Materials Chemistry of Bismuth *Tris*-(di-i-propylcarbamate): Deposition of Photoactive Bi_2O_3 Thin Films

Samuel D. Cosham, Michael S. Hill, Graeme A. Horley, Andrew L. Johnson, Laura Jordan, Kieran C. Molloy,* and David C. Stanton

Department of Chemistry, University of Bath, Claverton Down, Bath, BA2 7AY, U.K.

Supporting Information

ABSTRACT: The bismuth carbamate $Bi(O_2CNPr^i_2)_3$, a tetramer in the solid-state, has been synthesized and used to deposit mixtures of bismuth oxides by aerosol-assisted chemical vapor deposition (AACVD). The nature of the deposited oxide is a function of both temperature and run-time. Initially, δ-Bi_2O_3 is deposited, over which grows a thick layer of β-Bi_2O_3 nanowires, the latter having an increasing degree of preferred orientation at higher deposition temperatures. The photocatalytic activity of a thin film of δ-Bi_2O_3 for the degradation of methylene blue dye was found to be similar to that of a commercial TiO_2 film on glass, while the film overcoated with β-Bi_2O_3 nanowires was less active. Exposure of $Bi(O_2CNPr^i_2)_3$ to controlled amounts of moist air affords the novel oxo-cluster $Bi_8(O)_6(O_2CNPr^i_2)_{12}$, whose structure has also been determined.

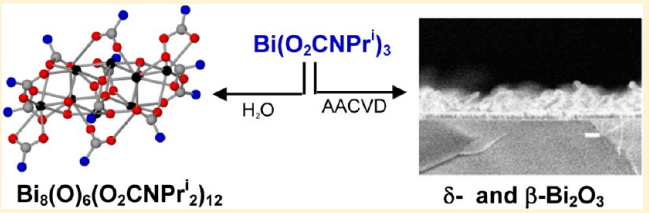

INTRODUCTION

Carbamates ($R_2NCO_2^-$) are an interesting class of ligand which form a link between carboxylates (RCO_2^-) and dithiocarbamates ($R_2NCS_2^-$). They have been widely studied as metal complexes across most of the Periodic Table,[1] though surprisingly only one brief report has appeared concerning bismuth.[2] Beyond the structural interest, carbamates (or isomers thereof) offer an alternative ligand for the formation of potentially volatile precursors for chemical vapor deposition (CVD),[3,4] and in this regard the two substituents on nitrogen offer additional opportunities for steric crowding, in comparison with, for example, carboxylates. Bismuth carbamates are, therefore, possible precursors for Bi_2O_3, a material exploited either alone[5] or, more significantly, as a component of more complex materials such as $Bi_2Sn_2O_7$ (catalyst, CO sensor),[6,7] $BiFeO_3$ (a multiferroic compound),[8] $Bi_4YTi_3O_{12}$ and $SrBi_2Ta_3O_9$ (ferroelectric perovskites),[9,10] and $Bi_2Sr_2CaCu_2O_8$ (high temperature superconductor).[11] Existing CVD precursors for bismuth oxides include BI_3,[12−18] $Bi(NO_3)_3$,[19] $BiPh_3$[20−22] and related bismuth aryls[23] and alkyls,[24] β-diketonates such as $Bi(thd)_3$ (thd = tetramethylheptane-dione),[23,25,26] and both simple and functionalized alkoxides,[27−29] all summarized in refs 5 and 28. However, of these only the three alkoxides[27−29] are single-source precursors (SSPs), the remainder requiring a co-reactant, usually O_2.

In this paper we report the first structural characterization of a bismuth carbamate, and its controlled hydrolysis to an unusual Bi_8-oxo cluster, along with use of the carbamate as a CVD precursor for photoactive Bi_2O_3 thin films.

EXPERIMENTAL SECTION

General Procedures. All operations were performed under an atmosphere of dry argon using standard Schlenk line and glovebox techniques. Hexanes were dried using a commercially available solvent purification system (Innovative Technology Inc., MA, U.S.A.) and degassed under argon prior to use. Tetrahydrofuran (THF) was dried by refluxing over potassium before isolating by distillation and degassing under argon prior to use. Deuterated benzene (C_6D_6) and deuterated chloroform ($CDCl_3$) NMR solvents were purchased from Fluorochem, U.K., and dried by refluxing over potassium and over 4 Å molecular sieves respectively, before isolating via vacuum distillation. All dry solvents were stored under argon in Youngs ampules over 4 Å molecular sieves. $BiCl_3$ and 2 M solution of $LiNPr^i_2$ (Acros Organics) were purchased from commercial sources and used as received. $Bi(NPr^i_2)_3$ was prepared by a literature procedure.[30]

Melting points were determined utilizing a Stuart SMP10 Melting Point Apparatus. Elemental analyses were performed externally by London Metropolitan University Elemental Analysis Service, U.K. Solution ^1H and $^{13}C\{^1H\}$ NMR spectra were recorded with a Bruker Avance 300 spectrometer at ambient temperature (25 °C). ^1H and ^{13}C NMR chemical shifts are referenced internally to residual non-deuterated solvent resonances. All chemical shifts are reported in δ (ppm) and coupling constants in hertz (Hz). The following abbreviations are used: d (doublet), m (multiplet), and br (broad).

Synthesis of $Bi(O_2CNPr^i_2)_3$ (1). Dry CO_2 was slowly bubbled through a stirred solution of $Bi(NPr^i_2)_3$ (0.51 g, 1 mmol) in hexanes (15 mL) for 30 min. Crystallization from the reaction solution at −28 °C yielded the desired product as small colorless crystals. Yield = 0.53 g, 83%.

Alternatively, the same compound can be prepared in a one-pot synthesis, as follows. A stirred suspension of $BiCl_3$ (8.51 g, 27 mmol) in THF (100 mL) was slowly treated at −78 °C with a 2 M THF/*n*-heptane/ethylbenzene solution of $LiNPr^i_2$ (42.0 mL, 84 mmol). The reaction solution was slowly allowed to warm to ambient temperature and stirred for 4 h, before volatiles were removed in vacuo. To the residue, hexanes (150 mL) were added, and the resultant solution filtered through Celite. Dry CO_2 was then slowly bubbled through the

Received: October 3, 2013
Published: December 10, 2013

   dx.doi.org/10.1021/ic402499r | Inorg. Chem. 2014, 53, 503−511

solution for 1 h, with subsequent crystallization from the reaction solution at −28 °C yielding the desired product as colorless crystals. Yield: 11.96 g, 69%. mp 91−92 °C. Analysis, found (calculated for $C_{21}H_{42}BiN_3O_6$): C 39.46 (39.31), H 6.52 (6.60), N 6.68 (6.55)%. ^{1}H NMR (300 MHz, C_6D_6): δ_H 3.92 (br m, 1H, C*H*CH$_3$), 1.28 (d, 6H, CHC*H*$_3$, $^3J_{CHCH3}$ 6.6). $^{13}C\{^1H\}$ NMR (75.5 MHz, C_6D_6): δ_C 163.6 (NCO_2), 45.9 (CH), 21.2 (CH_3).

Synthesis of $Bi_8(O)_6(O_2CNPr^i_2)_{12}$ (2). A hexanes solution containing **1** was prepared as described above before volatiles were subsequently removed in vacuo. The resultant residue was dissolved in THF (15 mL), and the solution was then filtered. Compound **2** was obtained as colorless crystals by crystallization from this reaction solution upon partial exposure to the ambient atmosphere for 72 h. Yield: 0.09 g, 21%. mp 204−208 °C (dec.). Analysis, found (calculated for $C_{84}H_{168}Bi_8N_{12}O_{30}$): C 28.81 (28.84), H 4.75 (4.84), N 4.77 (4.80)%. ^{1}H NMR (300 MHz, $CDCl_3$): δ_H 4.33−3.60 (br m, 3H, C*H*CH$_3$), 2.98−2.83 (m, 1H, C*H*CH$_3$), 1.23 (d, 6H, CHC*H*$_3$, $^3J_{CHCH3}$ 6.3), 1.19−1.07 (m, 12H, CHC*H*$_3$), 1.04 (d, 6H, CHC*H*$_3$, $^3J_{CHCH3}$ 6.2). $^{13}C\{^1H\}$ NMR (75.5 MHz, $CDCl_3$): δ_C 162.9, 161.8 (NCO_2), 45.3 (CH), 21.2, 21.1, 21.0 (CH_3).

Diffusion Ordered Spectroscopy (DOSY) NMR Procedure. Diffusion experiments were performed for 1 M and saturated solutions of **1** in dried d_8-toluene and were recorded at 298 and 353 K on a Bruker Avance 400 spectrometer operating at 400.13 MHz for ^{1}H. Experiments were performed using a double stimulated echo pulse sequence to allow for convection compensation, with Δ of 50 ms and δ of 2 ms. Gradient strengths were incremented linearly, in eight steps, from 1.74 to 33.14 G cm^{-1}, with 16 scans recorded at each gradient strength. Diffusion coefficients were calculated using Bruker's inbuilt T1/T2 software. The hydrodynamic radius (r) of **1** was calculated using the Stokes−Einstein equation:

$$r = \frac{k_B T}{6\pi\eta D}$$

where k_B is the Boltzmann constant, T is the temperature, η is the viscosity of the solution, and D is the diffusion coefficient.

Crystallography. Experimental details relating to the single-crystal X-ray crystallographic studies are summarized in Table 1. For both structures, data were collected on a Nonius Kappa CCD diffractometer at 150(2) K using Mo−K_α radiation (λ = 0.71073 Å). Structure solution followed by full-matrix least-squares refinement was performed using the WinGX-1.70 suite of programs.[31] Corrections for absorption (multiscan) were made in both cases. The asymmetric unit of **1** consists of one-quarter of the tetrameric complex and a co-crystallized solvent molecule at half occupancy. This latter has been modeled as pentane, though symmetry places two such molecules in close proximity. It is likely that the solvent present is a mixture of hexane isomers (see the synthetic protocol), though we have made no further effort to model this aspect of the structure given its relative unimportance. Bond lengths and angles in the solvent molecule have been geometrically fixed and C(35) is refined isotropically. **2**: The asymmetric unit contains three THF molecules (6 per Bi_8 cluster), one of which is disordered over two sites in a 87:13 ratio.

Table 1. Crystal Data and Structure Refinement for 1 and 2

identification code	**1**	**2**
empirical formula	$C_{94}H_{192}Bi_4N_{12}O_{24}$	$C_{108}H_{216}Bi_8N_{12}O_{36}$
formula weight	2710.52	3930.77
crystal system	tetragonal	monoclinic
space group	$P42_1c$	$P2_1/n$
a (Å)	19.5893(1)	16.1210(2)
b (Å)	19.5893(1)	27.1155(3)
c (Å)	15.6809(1)	16.8963(3)
β (deg)		105.4263(7)
V (Å^3)	6017.40(6)	7119.77(17)
Z	2	2
ρ_{calc} (Mg m^{-3})	1.496	1.834
μ(Mo-k$_\alpha$) (mm^{-1})	5.897	9.921
F(000)	2728	3800
crystal size (mm)	0.25 × 0.25 × 0.20	0.20 × 0.12 × 0.08
θ range	4.83 to 30.03 deg.	3.84 to 30.20 deg.
reflections collected	121369	93257
independent refl' [R(int)]	8761 [0.0611]	19721 [0.1093]
refl'ns observed (>2σ)	8163	13013
data completeness (%)	99.3	93.2
max., min transmission	0.3851, 0.3203	0.5041, 0.2416
goodness-of-fit on F^2	1.086	1.012
final R$_1$, wR$_2$ [I > 2σ(I)]	0.0228, 0.0546	0.0444, 0.0745
final R$_1$, wR$_2$ (all data)	0.0270, 0.0572	0.0965, 0.0864
Flack parameter	−0.035(5)	
largest diff. peak, hole (e Å^3)	2.270, −1.459	1.426, −1.711

Materials Chemistry. Thermogravimetric analyses (TGA) were performed either at SAFC HiTech, Bromborough, U.K., using a Shimadzu TGA-51 Thermogravimetric Analyzer (**1**), or at Bath using a TA Instruments Q500 TGA instrument (**2**). Data points were collected every second at a ramp rate of 10 °C min^{-1} in a flowing (90 mL min^{-1}) N_2 stream.

Film depositions were carried out at atmospheric pressure in a cold-wall Electrogas reactor containing a graphite heating block on which the substrate is situated. The precursor was injected as a 0.05 M hexanes solution (20 mL) into a glass flask sitting in an ultrasonic nebulizer, located just before the reactor chamber. Prior to injecting the precursor, the chamber was loaded with the substrate and heated under a flow of preheated nitrogen (0.8 L/min, 120 °C) to the required temperature before allowing it to equilibrate for at least 30 min. The precursor was then injected and the nebulizer started to initiate the deposition. Films were deposited on glass substrates at 300 °C for run times of 10 min (R1) and 40 min (R2), at 375 °C for 40 min (R3) and at 450 °C for 40 min (R4). After each deposition, the films were allowed to cool slowly to ambient temperature under a flow of nitrogen. The glass substrates (glass microscope slides) were cleaned via sonication in Piranha solution, rinsed with deionized water, and dried under a flow of N_2 prior to loading into the chamber.

Photocatalysis Studies. The photocatalytic activities of the δ- and β-Bi_2O_3 films were evaluated by the decolorization of methylene blue (MB). A 200 W HMI HR lamp (AM 1.5, 1 Sun, 735 W m^{-2}) was used as a light source to provide broad wavelength solar irradiation. The experiments were performed under ambient temperature as follows: In each run, the photoactive film (2.5 cm^2) was placed in a glass vessel and submerged in 10 mL of MB solution (1×10^{-5} mol L^{-1}). Before illumination, the solution was stirred for 30 min in the dark to equilibrate adsorption−desorption of MB and photocatalyst. The solution was then stirred and exposed to solar irradiation. The concentration of the MB was monitored by measurement of the absorbance at 665 nm during the photodegradation process using a Varian Cary 50 UV−visible spectrophotometer.

RESULTS AND DISCUSSION

Synthesis and Structural Chemistry. The homoleptic bismuth carbamate $Bi(O_2CNPr^i_2)_3$ (**1**) was synthesized by the insertion of CO_2 into the Bi−N bonds of $Bi(NPr^i_2)_3$.[30] On bubbling dry CO_2 through a green solution of $Bi(NPr^i_2)_3$ in hexanes, there is a color change to pale yellow over a period of about 15 min. Alternatively, the synthesis is also viable in "one pot", by mixing $BiCl_3$, $LiNPr^i_2$ and bubbling CO_2 through the mixture without isolation of the $Bi(NPr^i_2)_3$ intermediate. The NMR data of **1** are exceptional, showing the expected doublet/septet pattern for the i-Pr groups in the ^{1}H NMR and three resonances in the ^{13}C NMR (19.8, 44.4, 162.2 ppm), the most diagnostic of which is the latter signifying the formation of the sp^2 NCO_2 center.

Compound **1** is moderately air-sensitive and controlled exposure to moist air (by allowing a concentrated solution of **1**

dx.doi.org/10.1021/ic402499r | Inorg. Chem. 2014, 53, 503−511

to be exposed to the atmosphere over 2 days) leads to both the formation and crystallization of the oxo-cluster $Bi_8(O)_6(O_2CNPr^i_2)_{12}$ (**2**).

$$Bi(NPr^i_2)_3 \xrightarrow{CO_2} \underset{(\mathbf{1})}{Bi(O_2CNPr^i_2)_3}$$

$$\mathbf{1} \xrightarrow{\text{moist air}} \underset{(\mathbf{2})}{Bi_8(O)_6(O_2CNPr^i_2)_{12}}$$

The ^{1}H NMR spectrum of **2** is complex, but shows that there are two distinct CH and three distinct CH_3 environments which persist in solution arising from restricted rotation about the HC−CH_3 bonds of the peripheral i-Pr groups.

The structure of **1** is shown in Figure 1, along with some selected bond length data. Each bismuth is bonded to two chelating carbamate ligands while the remaining ligand bridges two metal centers. This leads to tetrameric species (Figure 2a), involving a non-planar sixteen-membered $(BiOCO)_4$ ring; the overall shape of the tetramer is that of a box with the lid removed (Figure 2b). The geometry at bismuth can be described as pentagonal bipyramidal, with the two Bi−O bonds associated with the bridging carbamate [Bi−O(5) 2.232(2), Bi−O(6′) 2.440(2) Å] occupying the axial sites and the bonds to the chelating carbamates, including two of the weaker interactions [Bi−O(2) 2.681(2), Bi−O(4) 2.553(2) Å], along with a void occupied by the lone pair, making up the equatorial girdle. The geometry is, however, severely distorted, with additional long contacts which merit discussion. First, an oxygen of one chelating ligand forms long contacts with the symmetry-related metals either side [O(2)···Bi′ 2.813(2); O(2)···Bi‴ 3.293(2) Å], of which only the shorter is shown in Figure 2a. There is a further long, chelating contact between bridging O(6) and bismuth [3.207(2) Å] but the orientation of the atoms makes this interaction marginal at best; such an interaction, but at 3.27 Å, has been noted in $Bi(O_2CBu^t)_3$.[32] Indeed, the structure **1** is comparable to that reported for $Bi(O_2CBu^t)_3$ in that it too exists as cyclic tetrameric units, with two terminal carboxylate ligands and one bridging carboxylate ligand per bismuth center. For comparison, in the carboxylate the oxygen which protrudes into the center of the "box" is at 2.87 and 3.16 Å from the nearest metals.[32]

The composition of **1** in solution has been probed by DOSY NMR.[33] For an ca. 1 M solution in d_8-toluene, the estimated molecular radius extracted from the diffusion coefficient using the Stokes−Einstein equation is 6.5 Å, which is broadly consistent with a monomeric unit taken from the structure of the tetramer (Bi... outer hydrogens ca. 6.5 Å), though this is

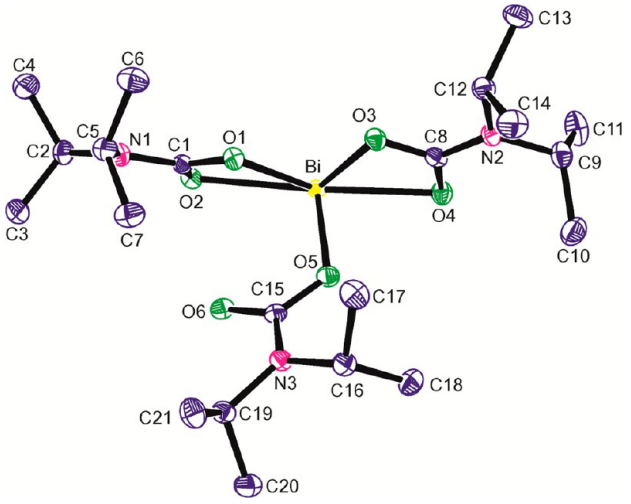

Figure 1. Asymmetric unit of **1** showing the labeling scheme used; thermal ellipsoids are at the 40% probability level. The co-crystallized, disordered solvent molecule, modeled as pentane, has been omitted for clarity. Selected metrical data: Bi−O(1) 2.217(2), Bi−O(2) 2.681(2), Bi−O(3) 2.227(2), Bi−O(4) 2.553(2), Bi−O(5) 2.232(2), Bi−O(6′) 2.440(2), Bi−O2‴ 2.813(2) Å.

Scheme 1

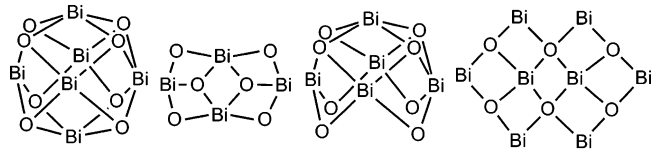

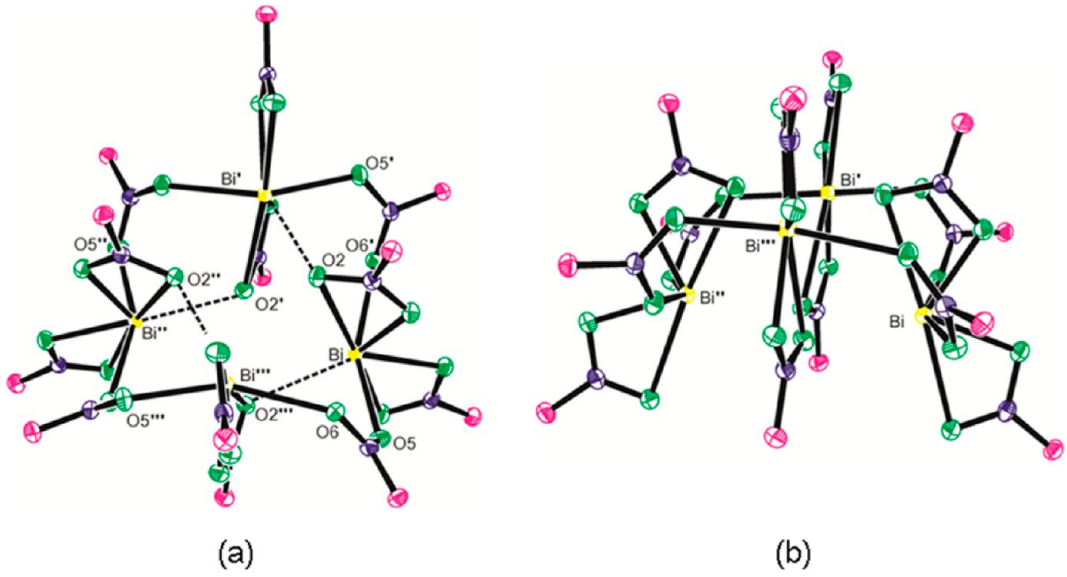

Figure 2. Two views of the tetrameric aggregation of **1** (a) showing weak intermolecular contacts between Bi and O2‴ and (b) the nonplanar nature of the ring. Symmetry operations: ′ *y*, 1−*x*, −*z*; ″ 1−*x*, 1−*y*, *z*; ‴ 1−*y*, *x*, 1−*z*.

dx.doi.org/10.1021/ic402499r | *Inorg. Chem.* 2014, 53, 503−511

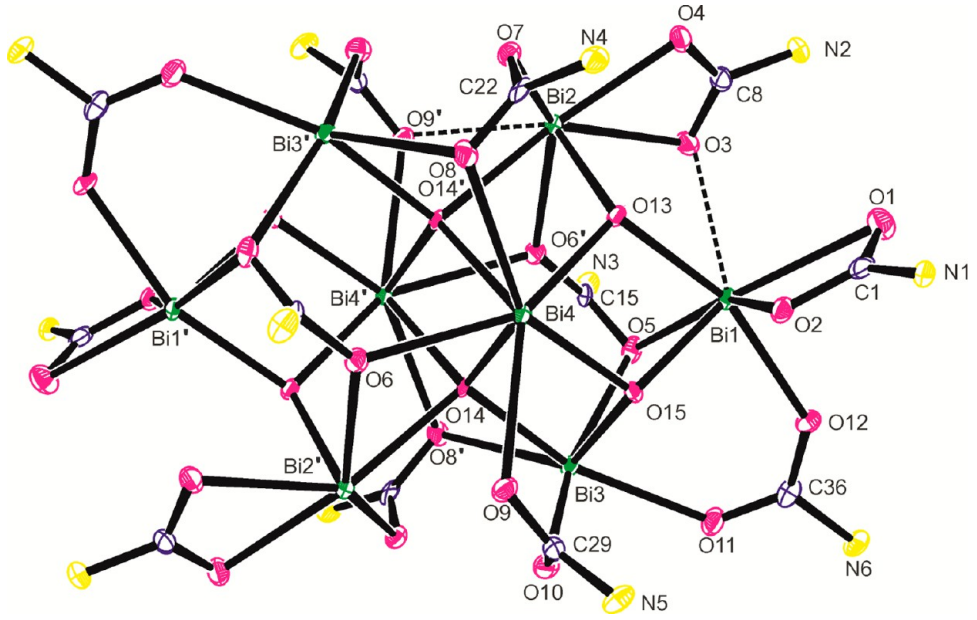

Figure 3. Asymmetric unit of **2** showing the labeling scheme used; thermal ellipsoids are at the 40% probability level. Selected metrical data: Bi(1)–O(1) 2.724(4), Bi(1)–O(2) 2.194(4), Bi(1)–O(3) 3.058(4), Bi(1)–O(5) 2.703(4), Bi(1)–O(12) 2.320(4), Bi(1)–O(13) 2.251(4), Bi(1)–O(15) 2.126(4), Bi(2)–O(3) 2.504(4), Bi(2)–O(4) 2.362(4), Bi(2)–O(6′) 2.520(4), Bi(2)–O(7) 2.327(4), Bi(2)–O(9′) 2.951(4), Bi(2)–O(13) 2.107(4), Bi(2)–O(14′) 2.488(4), Bi(3)–O(5) 2.456(4), Bi(3)–O(8′) 2.813(4), Bi(3)–O(10) 2.234(4), Bi(3)–O(11) 2.424(4), Bi(3)–O(14) 2.246(4), Bi(3)–O(15) 2.133(4), Bi(4)–O(6) 2.604(4), Bi(4)–O(8) 2.798(4), Bi(4)–O(9) 2.687(4), Bi(4)–O(13) 2.233(4), Bi(4)–O(14) 2.168(4), Bi(4)–O(14′) 2.284(4), Bi(4)–O(15) 2.289(4) Å. Symmetry operation: 1−*x*, 1−*y*, −*z*.

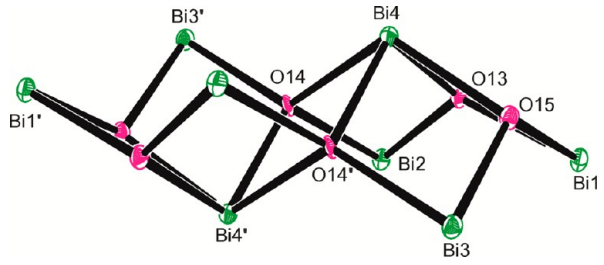

Figure 4. Bi_8O_6 core of **2**. Symmetry operation: 1−*x*, 1−*y*, −*z*.

probably an overestimate of the size of a more spherical tris-chelated monomer; for example, the radius of *tris*-(1-methoxy-2-methyl-2-propanolato-O,O′)bismuth(III) is in the range 4.4–5.1 Å.[34] Furthermore, the accuracy of radii derived from such DOSY measurements is open to question.[35] However, both the ^{1}H and ^{13}C NMR spectra only show one environment for the i-Pr groups at this concentration, which is also consistent with a *tris*-chelated monomer, though a more complex, but fluxional entity would also show this behavior. For comparison, a completely saturated solution shows very broad ^{1}H, ^{13}C NMR signals which may be indicative of some association of monomers. Analysis of the DOSY data for this solution is compromised by these broad signals and the tendency for the sample to start crystallizing from solution. The extrapolated molecular radius from the solution at 353 K (to minimize crystallization) is about 10 Å, though this assumes the viscosity of the solution is the same as pure d_8-toluene which may not be

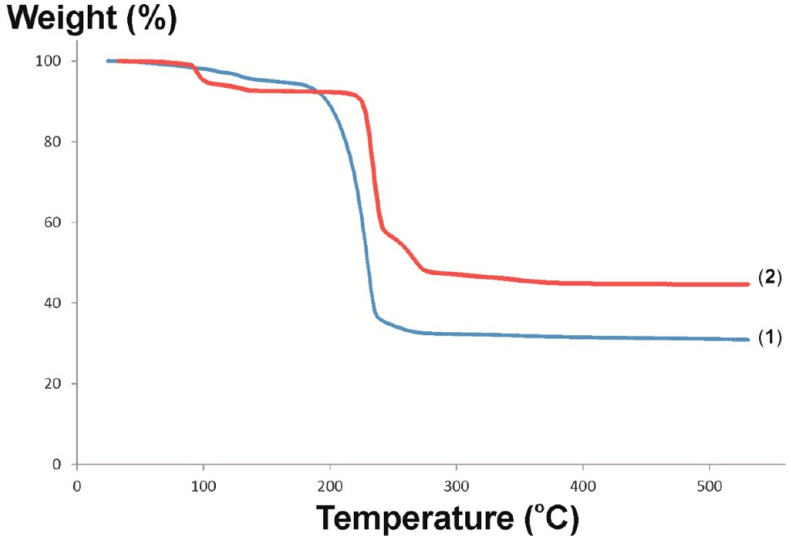

Figure 5. TGA of **1** and **2**.

dx.doi.org/10.1021/ic402499r | *Inorg. Chem.* 2014, 53, 503–511

true given the high concentration of solute. However, the collective data suggest that at high concentrations any equilibrium between a monomer and the tetramer seen in the solid state is moving toward the latter. It should be noted that the AACVD experiments were carried out on ca. 0.5 M solutions, and thus the "precursor species" is almost certainly a monomeric unit.

The structure of **2** comprises a Bi_8O_6 core supported by 12 carbamate ligands (Figure 3). The structure is complex, and comprises 4 distinct bismuth environments, 5 bonding modes for the carbamate ligands, and 2 types of oxo-bridges. Each of Bi(1), Bi(2), and Bi(4) is bonded to 6 oxygen atoms in a distorted coordination sphere, with space evident which is presumably occupied by a lone electron pair, though each metal also has an additional long Bi−O bond [Bi(1)−O(3): 3.058(4); Bi(2)−O(9′) 2.951(4), Bi(4)−O(8) 2.798(4) Å]. Bi(3) has 5 short and 1 long Bi−O bonds [Bi(3)−O(8′) 2.813(4) Å] again in a distorted coordination sphere with space occupied by a lone electron pair. Bi(1) is bonded to one chelating carbamate, one μ_2-bridging carbamate, one μ_3-bridging carbamate, one μ_4-bridging carbamate, and two oxo-ligands, while Bi(2) is similarly ligated but with the chelating carbamate replaced by a second μ_3-bridging ligand. Bi(3) is surrounded by four bridging carbamates (μ_2, two μ_3, μ_4) and two oxo-ligands, while Bi(4), at the heart of the cluster, is bonded to three carbamates (two μ_3, μ_4) and four lone oxygen atoms.

The carbamate ligands divide between those which are purely chelating [e.g., κ^2-O(1)/O(2)], of which there are two after symmetry considerations, those which bridge two metal centers [μ_2-O(11)/O(12), two in total], four which bridge three bismuths [μ_3-O(7)/O(8) and O(9)/O(10)], two which bridge between four metal centers [μ_4-O(5)/O(6) and its symmetry-related partner], and two which both chelate and bridge [μ_2, κ^2-O(3)/O(4)]; the oxo-ligands bridge metals in either a μ_3-[O(13,15)] or μ_4-manner [O(14)].

The overall geometry is too irregular to make anything other than general comments about the bond lengths. Thus, the Bi−O bonds to the μ_2-bridging carbamates [2.242(4), 2.320(4) Å] are generally shorter than those involving either the μ_4-carbamate ligands [2.456(4)−2.703(4) Å], though the bonds involving the μ_3-ligands are highly asymmetric [2.234(4), 2.327(4), 2.687(4)−2.951(4) Å]. Similarly, Bi−O(μ_3) tend to be shorter [2.107(4)−2.289(4) Å] than those involving the μ_4-O [2.168(4)−2.488(4) Å], though the situation is less clear-cut around Bi(4). The κ^2-ligand chelates vary asymmetrically [2.149(4), 2.724(4) Å], a situation which becomes more symmetrical in the μ_2,κ^2-ligand [2.362(4), 2.504(4) Å] when a long bridging interaction is added [3.058(4) Å].

Only two other examples of Bi_8-oxo clusters are cited in a recent review,[5] namely, $Bi_8(O)_4(OC_6F_5)_{16}$[36] and $Bi_8(O)_4$(*p*-Bucalix[8]-aren),[37] both of which show lower levels of hydrolysis than **2**; more recently, the structure of $Bi_4(OH)_4$(2,6-pdc)$_4(H_2O)_3{\cdot}H_2O$ has been reported (2,6-pdc = 2,6 pyridine dicarboxylate), which contains a linear $[Bi_8(2,6\text{-pdc})_8]^{8+}$ unit in which each metal is bridged by a $(2,6\text{-pdc})^{2-}$ ligand.[38] Small Bi−O clusters have been rationalized in terms of the building blocks **A**−**C** (Scheme 1), which in turn are generated from mononuclear μ_3-OBi_3 and μ_4-OBi_4 entities;[36] the aqueous chemistry of Bi salts is dominated by the octahedron of metals in **A** ($[Bi_6O_8]^{2+}$, a motif common to hydroxyl and alkoxy derivatives), and clusters with Bi_3, Bi_6, and Bi_9 are thus relatively common.[5] The structure of $Bi_8(O)_4(OC_6F_5)_{16}$ is derived from **A** by the addition of two, exo-octahedral bismuth atoms, converting two μ_3-OBi_3 units into μ_4-OBi_4.[36] $Bi_8(O)_4$(*p*-Bucalix[8]aren) is built from two **B** subunits (a common feature of many observed structures) rotated 90° to each other.[37] In contrast, the overall shape of **2** can be described as derived by the loss of one metal from **A** to generate the square-based pyramid of metals in **C** ($[Bi_5O_8]^-$), two of which, inverted with respect to each other, fuse sharing a common edge (Figure 4).

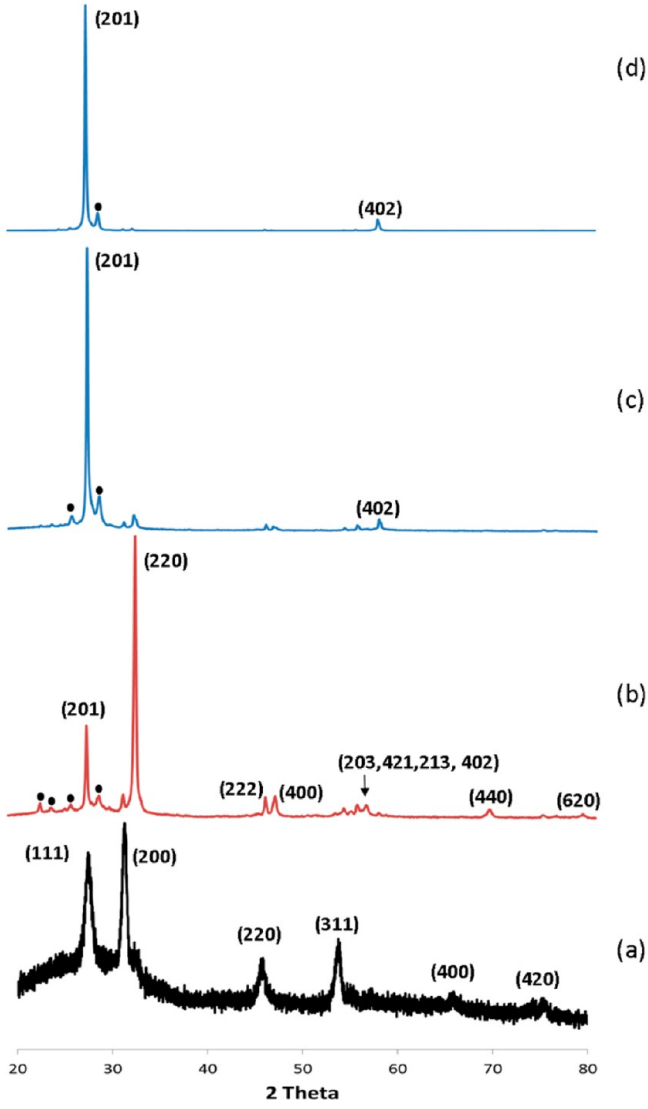

Figure 6. PXRD plots of the films grown from **1**; bottom upward (a) deposition at 300 °C for 10 min (R1), (b) deposition at 300 °C for 40 min (R2), (c) deposition at 375 °C for 40 min (R3), and (d) deposition at 450 °C for 40 min (R4). In (a), indexing is to cubic δ-Bi_2O_3 (PDF 77-2008), (b−d) indexed to tetragonal Bi_2O_3 (PDF 78-1793), with ● attributed to $Bi_2O_{2.73}$ (PDF 76-2477) and the residue of δ-Bi_2O_3 visible but unlabeled in (b).

In this respect, and in terms of formula, **2** is unique among the limited examples of other Bi_8 oxo-clusters as the schematic of the core (**D**) highlights. This motif can, however, be discerned within $[Bi_9(O)_8(OR)_6]^{5+}$[39] and the heterometallic cluster $Bi_{15}Na_3(O)_{18}(OSiMe_3)_{12}$.[40]

Materials Chemistry. Bismuth oxide is a remarkable material, occurring in five polymorphic forms (α, β, γ, δ, and ω) of which the α- and δ-forms are considered stable while the others are metastable.[41,42] Each modification has its own properties, for example, the bandgap for Bi_2O_3 ranges from 2.0 eV (amorphous) to 2.85 eV (α), while BiO has a bandgap of 3.31 eV;[41] other

dx.doi.org/10.1021/ic402499r | Inorg. Chem. 2014, 53, 503−511

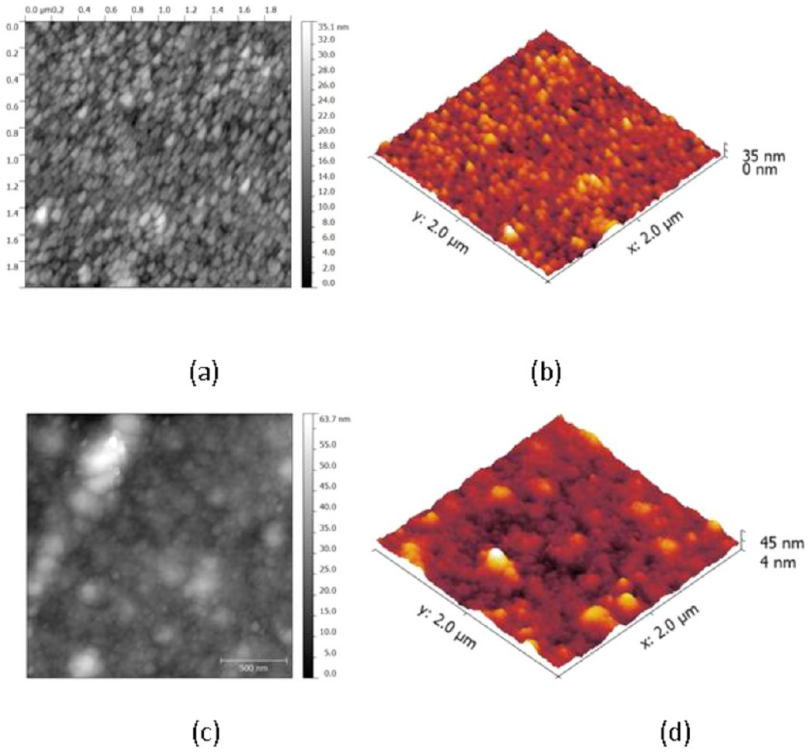

Figure 7. AFM analysis of the film grown from **1** at 300 °C after (a,b) 5 min and (c,d) 10 min deposition time. In each case the images cover a 2 × 2 μm region of the film.

authors report band gaps of 2.84–2.90 (α), 2.55–2.75 (β), 2.68–2.80 (γ), and 2.93–3.10 (δ)[43] though a wider spread of values than this can be found.[44]

The TGA of **1** and **2** is shown in Figure 5. For **1**, the residual mass at 300 °C (32.2%) is consistent with Bi_2O_3 formation (theoretical residual mass 34.4%), indeed the consistency is negatively compromised slightly by a small amount of residual solvent loss (ca. 2%) at the outset of the pyrolysis. Similarly, data for **2** show initial loss of lattice THF (theoretical loss for 6 THF per Bi_8 cluster 11.0%, observed 7.4% at 150 °C), the discrepancy probably arising from some loss of lattice THF on drying the material after synthesis; the %weight change between 150–400 °C (47.7%) is consistent with the transformation $Bi_8(O)_6(O_2CNPr^i_2)_{12} \rightarrow 4\ Bi_2O_3$ (theoretical % loss 46.7%).

Films of bismuth oxide have been deposited using **1** as precursor, by aerosol-assisted CVD (AACVD) onto glass substrates at temperatures between 300 and 450 °C (R1–R4) and the outcomes analyzed by powder X-ray diffraction (PXRD) (Figure 6), atomic force microscopy (AFM) (Figure 7), and scanning electron microscopy (SEM) (Figure 8). At 300 °C over a 10 min deposition time (R1), a hard, light brown/yellow, transparent film was produced which was strongly adhered to the glass substrate; PXRD can be indexed to the cubic δ-modification of Bi_2O_3 (Figure 6a). The film is smooth and featureless making it hard to image, but can be clearly seen in the SEM (edge view) of the film grown at the same temperature over a longer period (Figure 8a; see below) and is about 300 nm in thickness. This is in marked contrast to the elaborate hierarchical structures obtained by base hydrolysis of $Bi(NO_3)_3$/NH_4VO_3 mixtures.[45] AFM analysis of this growing film shows that, after 5 min the film comprises particles of dimension about 20 nm (Figure 7a,b), which become less well-defined after 10 min growth time (Figure 7c,d); the estimated roughness of the films is about 6 nm. A similar morphology has been observed

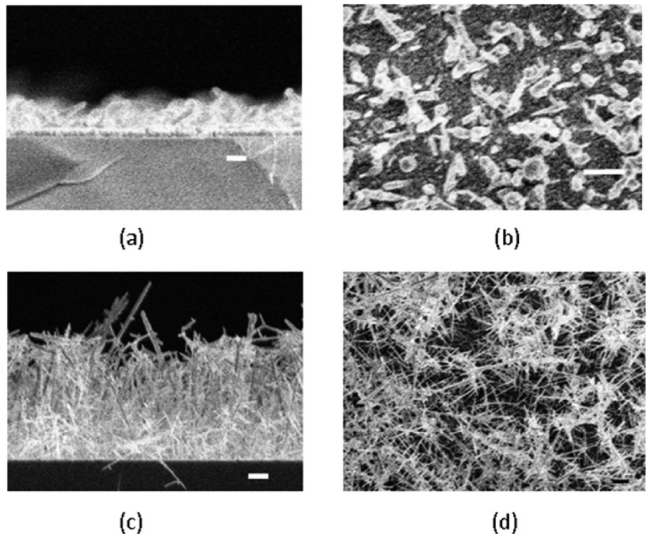

Figure 8. SEM of the films grown from **1**, (a,b) at 300 °C for 40 min (R2) and (c,d) at 450 °C for 40 min (R4); bar = 1 μm in all images.

for β-Bi_2O_3 grown by dip coating a solution of $Bi(NO_3)_3$/2-methoxyethanol and the organic template $(CH_2CH_2)_{0.67}$-$(CH_2CHCH_2CH_3)_{0.33}]_{89}(OCH_2CH_2)_{79}OH$ and calcined at 400 °C.[46]

When the run time is extended to 40 min (R2), the film has a more powdery, bright yellow appearance and is poorly adhered to the glass. The PXRD is dominated by reflections which can be indexed to tetragonal β-Bi_2O_3 with some preferential orientation in the (220) direction, this latter reflection appearing significantly more intense than that of (201), the dominant line in the random pattern; the underlying δ-Bi_2O_3 is still visible in the PXRD pattern, along with traces of substoichiometric

dx.doi.org/10.1021/ic402499r | Inorg. Chem. 2014, 53, 503–511

Table 2. Bi_2O_3 Phases and Deposition Temperatures for CVD-Grown Bismuth Oxide[a]

	BI_3/O_2	$BiPh_3/O_2$	$BiMe_3/O_2$	$Bi(thd)_3/O_2$	$Bi(OCMe_2Et)_3$	$Bi(OBu^t)_3$	**1** (this work)
200				amorphous[26,b]			
250				α[26,b]			
300				amorphous[25]			$\beta + \delta$[c,d]
375							β[d]
400		β[20]					
420, 425		$\alpha + \beta$[22,e]				β[28]	
450		γ + trace β[20,f]	α[24]	β[23]		α,β,γ[28,e]	β[d]
400–750							
500		α[20]					
550				α[25]			
600					α, γ[29]		
600–800	$Bi_2O_{2.33}$[12]						
700				γ[26,b]			
800	δ[14–16,18]						

[a]Deposition or annealing temperature depending on when the sample was analyzed by PXRD. [b]ALD. [c]Time dependent. [d]Traces $Bi_2O_{2.73}$ are also seen. [e]Product depends on gas flow rate, co-reactant H_2O. [f]o,p-$(CH_3C_6H_4)_3Bi$ deposit β modification at 450 °C.[23]

$Bi_2O_{2.73}$ (Figure 6b). SEM of this film (Figure 8a,b) show both the hard underlying δ-Bi_2O_3 (ca. 300 nm thick) and the growth of a more needle-like material above it (ca. 1 μm in height). It would seem that at 300 °C the formation of δ-Bi_2O_3 provides a template on which β-Bi_2O_3 grows. At 375 °C (R3) and 450 °C (R4), only β-Bi_2O_3 is visible in the PXRD (save for traces of $Bi_2O_{2.73}$), with an increasing degree of preferred (201) orientation as the temperature is raised (Figures 6c, d). The base film of δ-Bi_2O_3 is still discernible in the image of the film grown at 450 °C (though it is now in such a relatively small amount as to not register in the PXRD of Figure 6d), which is now dominated by β-Bi_2O_3 fibers growing to about 5 μm in height (Figure 8c,d). Similar β-Bi_2O_3 nanowires have been deposited on aluminum at 300 °C by O_2 oxidation of bismuth powder heated to 800 °C over an 8 h period under an N_2 flow; however, under the same conditions at a substrate temperature of 500 °C the α-modification is formed.[47]

The most stable modifications of Bi_2O_3 are monoclinic α (up to 729 °C) and cubic δ (stable up to 824 °C), with metastable β- and γ-forms appearing on cooling at T ca. 600–650 °C.[48] However, CVD produces all four modifications across a range of temperatures, in which the modification adopted seems to depend on the precursor rather than temperature control (Table 2). Deposition using **1** affords the δ-modification, an excellent oxide ion conductor and the phase with the highest conductivity,[49] at the lowest temperature yet reported, with no evidence for the formation of either the α- or γ-modifications. The β-modification, which is dominant at both higher temperatures and at lower temperatures over an extended run time, also has good oxide ion conductivity, surpassing that of yttria-stabilized zirconia (YST). The formation of small amounts of substoichiometric $Bi_2O_{2.73}$ is, perhaps, not surprising given **1** is acting as a true SSP.

The photocatalytic activity of bismuth oxide is well documented, with α-,[47,50–52] β-,[46,47,52–55] and δ-polymorphs[45] being active, though the β-modification is considered the most active. In this work, single-phase δ-Bi_2O_3 has been assessed by the degradation of MB dye; a parallel experiment under similar conditions was carried out using a commercially marketed sample of TiO_2 on glass (NSG/Pilkington Activ) for comparison (Figure 9).

The 300 nm thin film of δ-Bi_2O_3 deposited from **1** over a 10 min period at 300 °C (R1, above) shows a very similar level

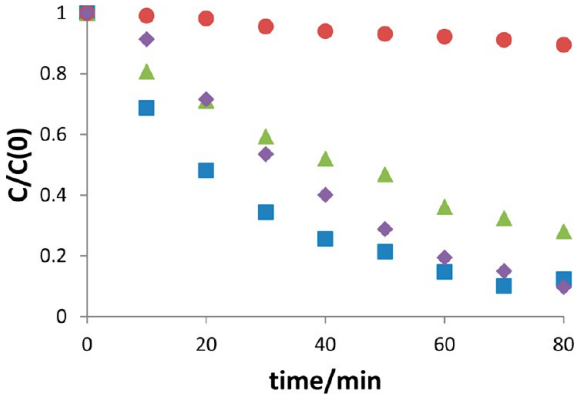

Figure 9. Photodegradation of only MB dye (red circles), MB dye using (purple diamonds) TiO_2 (NSG/Pilkington Activ), (blue squares) δ-Bi_2O_3 thin film, and (olive green triangles) δ-Bi_2O_3 thin film overcoated with β-Bi_2O_3 nanowires, all under a 200 W HMI HR lamp; C = concentration, C(0) = concentration at time 0 s.

of photocatalytic activity to commercial TiO_2-coated glass, while, in contrast, that of the film deposited over a 40 min period at 450 °C–β-Bi_2O_3 nanowires grown over the same δ-Bi_2O_3 base (R4, above; Figure 8c,d) were less active. It was noted that (i) despite their visual fragility the majority of nanowires appear to remain adhered to the underlying δ-Bi_2O_3 film during the photodegradation experiment, but (ii) the wettability of the nanowires was significantly less than that of the δ-Bi_2O_3 film, as reflected in contact angles of 73° and 137° for the δ- and β-Bi_2O_3 films, respectively (Figure 10). Thus it seems likely that the lower photoactivity of the β-Bi_2O_3

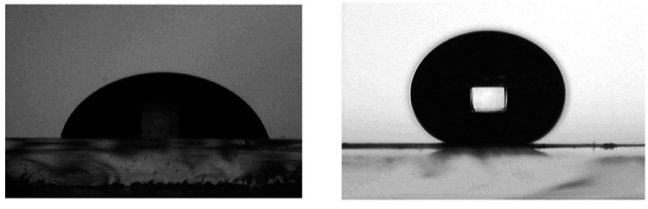

Figure 10. Contact angles of a water droplet on (a) δ-Bi_2O_3 (b) β-Bi_2O_3.

dx.doi.org/10.1021/ic402499r | Inorg. Chem. 2014, 53, 503–511

nanowires seems to be related to the poor interface between the catalyst and the aqueous solution in this system, which in turn can be attributed to the morphology of the as-deposited material.

CONCLUSIONS

The bismuth carbamate $Bi(O_2CNPr^i_2)_3$ (**1**) has proved a versatile precursor for the deposition of differing modifications of Bi_2O_3 films on glass, depending on the duration and temperature of the deposition process, providing a degree of control between δ- and β-Bi_2O_3. The δ-Bi_2O_3 films show good catalytic activity (comparable to commercial TiO_2 NSG/Pilkington Activ), and better than that of the deposited β-Bi_2O_3 nanowires, which have a much higher water droplet contact angle. Controlled exposure of **1** to atmospheric moisture yields the novel octa-bismuth cluster $Bi_8(O)_6(O_2CNPr^i_2)_{12}$ (**2**).

ASSOCIATED CONTENT

Supporting Information

Crystallographic data for the structural analysis (in CIF format). This material is available free of charge via the Internet at http://pubs.acs.org. The crystallographic data has also been deposited with the Cambridge Crystallographic Data Centre, CCDC nos. 940280, 940281 for **1**, **2**, respectively. Copies of this information may be obtained from the Director, CCDC, 12 Union Road, Cambridge, CB21EZ, U.K. (Fax: +44−1233−336033; e-mail: deposit@ccdc.cam.ac.uk or www.ccdc.cam.ac.uk).

AUTHOR INFORMATION

Corresponding Author

*E-mail: chskcm@bath.ac.uk.

Notes

The authors declare no competing financial interest.

ACKNOWLEDGMENTS

We thank Dr. John Lowe (University of Bath) for help with the DOSY experiments and Dr. Andrew Kingsley (SAFC HiTech) for recording the TGA of **1**.

REFERENCES

(1) Belli Dell'Amico, D.; Calderazzo, F.; Labella, L.; Marchetti, F.; Pampaloni, G. *Chem. Rev.* **2003**, *103*, 3857.
(2) Ando, F.; Hayashi, T.; Ohashi, K.; Koketsu, J. *J. Inorg. Nucl. Chem.* **1975**, *37*, 2011.
(3) Petrella, A. J.; Deng, H.; Roberrs, N. K.; Lamb, R. N. *Chem. Mater.* **2002**, *14*, 4339.
(4) Pothiraja, R.; Milanov, A. P.; Barreca, D.; Gasparotto, A.; Becker, H.-W.; Winter, M.; Fischer, R. A.; Devi, A. *Chem. Commun.* **2009**, 1978.
(5) Mehring, M. *Coord. Chem. Rev.* **2007**, *251*, 974.
(6) Wu, J.; Huang, F.; Chen, P.; Wan, D.; Xu, F. *J. Mater. Chem.* **2011**, *21*, 3872.
(7) Andrews, P. C.; Junk, P. C.; Nuzhnaya, I.; Thielemann, D. T. *Inorg. Chem.* **2012**, *51*, 751.
(8) Palai, R.; Scott, J. F.; Katiyar, R. S. *Phys. Rev. B* **2010**, *81*, 064110.
(9) Kang, S. W.; Rhee, S. W. *J. Mater. Sci.: Mater. Electron.* **2004**, *15*, 231.
(10) Kang, S. W.; Yang, K. J.; Yong, K. J.; Rhee, S. W. *J. Electrochem. Soc. India* **2002**, *149*, C44.
(11) Raffy, H. In *High-temperature superconductors*; Qui, X. G., Ed.; Woodhead: Cambridge, U.K., 2012.
(12) Schuisky, M.; Harsta, A. *Chem. Vapor Depos.* **1996**, *2*, 235.
(13) Takeyama, T.; Takahashi, N.; Nakamura, T.; Ito, S. *Opt. Mater.* **2004**, *26*, 413.
(14) Takeyama, T.; Takahashi, N.; Nakamura, T.; Ito, S. *J. Phys. Chem. Solids* **2004**, *65*, 1349.
(15) Takeyama, T.; Takahashi, N.; Nakamura, T.; Itoh, S. *J. Cryst. Growth* **2005**, *277*, 485.
(16) Takeyama, T.; Takahashi, N.; Nakamura, T.; Itoh, S. *J. Cryst. Growth* **2005**, *275*, 460.
(17) Takeyama, T.; Takahashi, N.; Nakamura, T.; Itoh, S. *Solid State Commun.* **2005**, *133*, 771.
(18) Takeyama, T.; Takahashi, N.; Nakamura, T.; Itoh, S. *Surf. Coat. Technol.* **2006**, *200*, 4797.
(19) Soitah, T. N.; Yang, C.; Yu, Y.; Niu, Y.; Sun, L. *Curr. Appl. Phys.* **2010**, *10*, 1372.
(20) Bedoya, C.; Condorelli, G. G.; Anastasi, G.; Baeri, A.; Scerra, F.; Fragala, I. L.; Lisoni, J. G.; Wouters, D. *Chem. Mater.* **2004**, *16*, 3176.
(21) Reuge, N.; Dexpert-Ghys, J.; Caussat, B. *Chem. Vapor Depos.* **2010**, *16*, 123.
(22) Bandoli, G.; Barreca, D.; Brescacin, E.; Rizzi, G. A.; Tondello, E. *Chem. Vapor Depos.* **1996**, *2*, 238.
(23) Bedoya, C.; Condorelli, G. G.; Finocchiaro, S. T.; Di Mauro, A.; Fragala, I. L.; Cattaneo, L.; Carella, S. *Chem. Vapor Depos.* **2005**, *11*, 261.
(24) Kim, H. W.; Myung, J. H.; Shim, S. H.; Lee, C. *Appl. Phys. A: Mater. Sci. Process.* **2006**, *84*, 187.
(25) Kang, S. W.; Rhee, S. W. *Thin Solid Films* **2004**, *468*, 79.
(26) Shen, Y. D.; Li, Y. W.; Li, W. M.; Zhang, J. Z.; Hu, Z. G.; Chu, J. H. *J. Phys. Chem. C* **2012**, *116*, 3449.
(27) Williams, P. A.; Jones, A. C.; Crosbie, M. J.; Wright, P. J.; Bickley, J. F.; Steiner, A.; Davies, H. O.; Leedham, T. J.; Critchlow, G. W. *Chem. Vapor Depos.* **2001**, *7*, 205.
(28) Moniz, S. J. A.; Blackman, C. S.; Carmalt, C. J.; Hyett, G. *J. Mater. Chem.* **2010**, *20*, 7881.
(29) Matchett, M. A.; Chiang, M. Y.; Buhro, W. E. *Inorg. Chem.* **1990**, *29*, 358.
(30) Vehkamaki, M.; Hatanpaa, T.; Ritala, M.; Leskela, M. *J. Mater. Chem.* **2004**, *14*, 3191.
(31) Farrugia, L. J. *J. Appl. Crystallogr.* **1999**, *32*, 837.
(32) Troyanov, S. I.; Pisarevskii, A. P. *Chem. Commun.* **1993**, 335.
(33) Ward, A. L.; Buckley, H. L.; Lukens, W. W.; Arnold, J. *J. Am. Chem. Soc.* **2013**, *135*, 13965.
(34) Williams, P. A.; Jones, A. C.; Crosbie, M. J.; Wright, P. J.; Bickley, J. F.; Steiner, A.; Davies, H. O.; Leedham, T. J.; Critchlow, G. W. *Chem. Vap. Deposition* **2001**, *7*, 205.
(35) Evans, R.; Deng, Z.; Rogerson, A. K.; McLachlan, A. S.; Richards, J. J.; Nilsson, M.; Morris, G. A. *Angew. Chem., Int. Ed.* **2013**, *52*, 3199.
(36) Whitmire, K. H.; Hoppe, S.; Sydora, O.; Jolas, J. L.; Jones, C. M. *Inorg. Chem.* **2000**, *39*, 85.
(37) Liu, L.; Zakharov, L. N.; Rheingold, A. L.; Hanna, T. A. *Chem. Commun.* **2004**, 1472.
(38) Zhang, X.-P.; Tian, H.-R.; Yan, G.-F.; Su, Y.; Feng, Y.-L.; Cheng, J.-W. *Dalton Trans.* **2012**, *42*, 1088.
(39) Thurston, J. H.; Swenson, D. C.; Messerle, L. *Chem. Commun.* **2005**, 4228.
(40) Mehring, M.; Paalasmaa, S.; Schürmann, M. *Eur. J. Inorg. Chem.* **2005**, 4891.
(41) Leontie, L.; Caraman, M.; Alexe, M.; Harnagea, C. *Surf. Sci.* **2002**, *507−510*, 480.
(42) Harwig, H. A. *Z. Anorg. Allg. Chem.* **1978**, *444*, 151.
(43) Li, E.; Lang, C.; Qiang, Z.; Wenhua, L.; Shuangfeng, Y. *Prog. Chem.* **2010**, *22*, 2282.
(44) Sirota, B.; Reyes-Cuellar, J.; Kohli, P.; Wang, L.; McCarroll, M. E.; Aouadi, S. M. *Thin Solid Films* **2012**, *520*, 6118.
(45) Zhou, L.; Wang, W.; Xu, H.; Sun, S. C.; Shang, M. *Chem.—Eur. J.* **2009**, *15*, 1776.
(46) Brezesinski, K.; Ostermann, R.; Hartmann, P.; Perlich, J.; Brezesinski, T. *Chem. Mater.* **2010**, *22*, 3079.

(47) Qiu, Y.; Yang, M.; Fan, H.; Zuo, Y.; Shao, Y.; Xu, Y.; Yanga, X.; Yang, S. *CrystEngComm* **2011**, *13*, 1843.
(48) Shuk, P.; Wiemhöfer, H.-D.; Guth, U.; Göpel, W.; Greenblatt, M. *Solid State Ionics* **1996**, *89*, 179.
(49) Harwig, H. A.; Gerards, A. G. *J. Solid State Chem.* **1978**, *26*, 265.
(50) Iyyapushpam, S.; Nishanthi, S. T.; PthinettamPadiyan, D. *Mater. Lett.* **2012**, *86*, 25.
(51) Muruganandham, M.; Amutha, R.; Lee, G.-J.; Hsieh, S.-H.; Wu, J. J.; Sillanpaa, M. *J. Phys. Chem. C* **2012**, *116*, 12906.
(52) He, W.; Qin, W.; Wu, X.; Ding, X.; Chen, L.; Jiang, Z. *Thin Solid Films* **2007**, *515*, 5362.
(53) Schlesinger, M.; Schulze, S.; Hietschold, M.; Mehring, M. *Dalton Trans.* **2013**, *42*, 1047.
(54) Zhong, J. B.; He, X. Y.; Li, J. Z.; Zeng, J.; Lu, Y.; Hu, W. *J. Adv. Oxid. Technol.* **2012**, *15*, 334.
(55) Schlesinger, M.; Weber, M.; Schulze, S.; Hietschold, M.; Mehring, M. *ChemistryOpen* **2013**, *2*, 146.